PHYSICS AND CHEMISTRY OF SOLID STATE
V. 22, No. 2 (2021) pp. 195-203
Section: Chemistry

DOI: 10.15330/pcss.22.2.195-203

Vasyl Stefanyk Precarpathian National University

ФІЗИКА І ХІМІЯ ТВЕРДОГО ТІЛА
Т. 22, № 2 (2021) С. 195-203
Хімічні науки

UDC: 549.731.11 ISSN 1729-4428

T. Tatarchuk[1], M. Myslin[1], I. Lapchuk[1], O. Olkhovyy[2], N. Danyliuk[1], V. Mandzyuk[1]

Synthesis, Structure and Morphology of Magnesium Ferrite Nanoparticles, Synthesized Via "Green" Method

[1]*Vasyl Stefanyk Precarpathian National University, Ivano-Frankivsk, 76018, Ukraine, tatarchuk.tetyana@gmail.com*
[2]*Jagiellonian University, Medyczna 9, 30-688 Kraków, oolkhovyi@gmail.com*

In this paper, the synthesis of spinel magnesium ferrite ($MgFe_2O_4$) nanoparticles is reported, along with its structural, magnetic and hyperthermic properties, which ensure them being effectively used in various fields. Firstly, magnesium ferrite was synthesized via sol-gel auto-combustion method, using honey as the reducing agent. The crystallite size was calculated via the Scherrer method, the modified Scherrer method, the Williamson-Hall method, and the size-strain plot (SSP) method. X-ray analysis was used to confirm the structure of the spinel. For morphological study of ferrite nanoparticles, scanning electron microscopy (SEM) was used. Finally, hyperthermic properties of magnesium ferrite were analyzed for potential usage in medicine. According to these results, spinel magnesium ferrite ($MgFe_2O_4$) nanoparticles proved to be suitable for destruction of cancer cells, as they can be heated to the desired temperature, which will increase the sensitivity of those cells.

Key words: spinel; magnesium ferrite; nanoparticles; "green" synthesis; magnetic hyperthermia.

Received 1 March 2021; Accepted 2 April 2021.

Introduction

Spinels are being actively studied and are not losing popularity among scientists. The term "spinel" characterizes a cubic structure with the general formula AB_2O_4, where ions A form a tetrahedral (8 ions A) and ions B – octahedral (16 ions B) sublattices. The main representatives of spinels are ferrites – oxides of transition metals, in which tetrahedrons contain cations of divalent metals (Mg^{2+}, Co^{2+}, Zn^{2+}), and octahedrons are represented by trivalent Fe^{3+} [1]. The distribution of cations on the sublattices forms three types of spinel structures – normal, inverse and mixed, which affect the properties of nanomaterials [2]. Therefore, depending on the structure, cationic composition, morphology of the particles – ferrites are characterized by optical, magnetic, adsorption and catalytic properties, which provide them with a wide range of applications in different fields [3, 4]. Due to their functional characteristics, spinels have been studied for various biomedical and medical applications, including cancer hyperthermia and magnetic resonance imaging [5]. Furthermore, ferrites are being widely used for the production of gas sensors, condensers, humidity sensors, inductors, magnetic fluids, microwave devices, catalysts, and also in telecommunications and electronics. Numerous studies see spinel nanoparticles being used for wastewater treatment because they are suitable for the removal of various contaminants, highly stable, and can be reused several times without losing their properties [3, 6]. Therefore, the widespread use of spinels leads to a more detailed study of individual representatives of ferrites, such as $MgFe_2O_4$, $ZnFe_2O_4$, $NiFe_2O_4$, $MnFe_2O_4$, $CoFe_2O_4$ et cetera [7].

Among the mentioned ferrite nanoparticles, $MgFe_2O_4$ is an important one, with a spinel structure, that can be used in catalysis, magnetic technology, manufacture of sensors [8]. Additionally, a study [9] showed the use of magnesium ferrite as anode materials for lithium-ion batteries. $MgFe_2O_4$ – nanoparticles of spinel ferrite with a cubic structure, where the tetrahedral and octahedral sublattices are aligned and occupied by divalent Mg^{2+} and trivalent Fe^{3+} [10]. Fe^{3+} ion of the spinel demonstrates typical magnetic properties due to high cation diffusion [11]. Magnesium ferrite shows low saturation magnetization, high resistance and stability, non-toxicity

[12]. Research shows that reducing the size of crystallites increases their specific surface area and enhances structural, magnetic and optical properties. This proves the shape, size and the method of synthesis of ferrite to be important for the characteristics and subsequent use of the spinel [13].

The widespread use of spinel nanomaterials has inspired the search and development of various methods of synthesis, each of them having certain advantages and disadvantages. These methods include: hydrothermal method [12], co-precipitation [14], solvothermal method [15], microemulsion method [16], thermal decomposition [17], sol-gel method [18], electrochemical method [19], ultrasonic (sonochemical) method [20]. Also, methods of "green" synthesis, which are environmentally friendly and safe, with a minimum amount of chemical waste, which meet the principles of green chemistry, are well-known in the research [21]. The concept of "green" chemistry is characterized by reducing or eliminating the use of hazardous substances in production processes, aiming to minimize threats to public health and the environment from toxic waste. This means that in the process of "green" synthesis biological materials, such as various plants or microorganisms should be used [22]. Therefore, obtaining nanomaterials using this method is a successful alternative process, and the use of natural plant extracts or other biological components makes this process more environmentally friendly and cost-effective [23].

Various bioreagents are being used for the "green" synthesis of nanoparticles. For example, Manik et al. [24] studied the effect of two plant leaf extracts - Artocarpus heterophylus and Azadirachta indica as reducing and stabilizing agents on the synthesis of silver nanoparticles. As a result, particles with a size of 20 - 40 nm were obtained, which can be used in cosmetics and pharmaceuticals. Vidovix et al. [25] extracted copper oxide via "green" synthesis method, with the addition of Punica pomegranate leaf extract. Such a nanomaterial with a spherical shape and a particle size of about 20 nm was subsequently used for adsorption of the methylene blue dye.

Maheshwaran et al. [26] showed the synthesis of silver oxide nanoparticles using a reducing agent – Zephyranthes Rosea (Z. rosea) flower extract. Particle size of about 10 – 30 nm and spherical morphology of Ag_2O were observed in the studies. Thangamani et al. [27] obtained Au nanoparticles (size < 10 nm) using Simarouba glauca leaf extract at different concentrations. Results showed the gold, synthesized via "green" method, to have excellent antimicrobial activity.

Apart from the mentioned nanoparticles, oxides obtained via "green" synthesis are quite actively being studied. Abdullah et al. [28] used date (Pheonix dactylifera) leaf extract in order to obtain stable Fe_2O_3 and Fe_3O_4 iron oxides with the size of 2 – 30 nm. These compounds were found to exhibit antioxidant activity, which increases with decreasing particle size. Aqueous extract of Himalayan cedar (Cedrus deodara) as an ecological and compatible reductant for obtaining copper oxide was used by Ramzan et al. [29]. In the process of synthesis after homogenization of the mixture of salt and extract, there was a color change from green to dark brown, which characterized the formation of oxide nanoparticles. Theophil Anand et al. [30] presented the production of zinc oxide using almond extract (Prunus dulcis). The calculated size of nanoparticles according to the Scherrer formula is equal to ~30 nm, the SEM image showed an almost spherical shape of nanoparticles with an even distribution, which significantly affects their antimicrobial properties.

Spinel ferrites obtained via "green" synthesis using biological components also show good magnetic, structural and optical properties. As an example, $ZnFe_2O_4$ nanoparticles were synthesized by Yadav et al. [31] using honey. The process involved the formation of a very viscous gel, which was being heated to 350 °C to initiate a combustion reaction with the subsequent formation of ferrite powder. Studies have shown that the particle size depended on the spinel annealing temperature: 30 - 60 nm at a lower temperature, 50 - 400 nm at a higher temperature. In the study by Laokul et al. [32], the size of MFe_2O_4 crystallites (where M = Cu, Ni and Zn) increased with increasing annealing temperature (range of 15 - 70 nm), and metal nitrates with Aloe vera solution extract were used for ferrite synthesis.

Thus, the ecological and cost-effective method of "green" synthesis for obtaining nanomaterials with functional properties is being actively studied by scientists and demonstrates good research results. The aim of this work is to synthesize the magnesium ferrite nanoparticles via "green" method using honey and to characterize its structure, morphology and hyperthermic parameters.

I. Materials and methods

1.1. Synthesis of magnesium ferrite

Magnesium ferrite was synthesized via sol-gel auto-combustion method, using honey, a substance of natural origin, as the reducing agent. $Mg(NO_3)_2 \cdot 6H_2O$ and $Fe(NO_3)_3 \cdot 9H_2O$ were also among the reagents. During the calculations, the ratio of oxidants to reductants was initially 1:1, meaning the stoichiometric coefficient (ϕ_e) was equal to 1. In order to calculate the charges of the reagents, the charges of the elements were taken into account ($V_C = 4$; $V_H = 1$; $V_O = -2$; $V_N = 0$; $V_{Me} = 2$ or 3). The required amount of honey for the synthesis was calculated, taking the oxygen balance equation into consideration. Since honey contains about 75 % of sugars (mainly fructose and glucose) as well as other substances, such as proteins, acids, enzymes, water, dextrins, vitamins and minerals, the honey for the synthesis was taken with a certain excess. The calculated amount of honey was dissolved in 75 ml of warm distilled water. Stoichiometric amounts of metal nitrates were dissolved in 75 ml of distilled water and homogenized for 30 min on a magnetic stirrer. Then, a solution of honey was added and homogenized for 30 min while being heated to 50 – 60 ºC. After, the solution was transferred to the tile and continued being heated. The solution turned into a sol, then into a gel and ignited spontaneously with the formation of $MgFe_2O_4$ magnetic powder. The sample was ground in a mortar and washed with warm water to get rid of soot. The process is described by the following reaction equation:

$$Mg(NO_3)_2 + 2\,Fe(NO_3)_3 + 4\frac{1}{3}C_6H_{12}O_6 + 16O_2 \rightarrow$$

$\rightarrow MgFe_2O_4 + 4N_2\uparrow + 26CO_2\uparrow + 26H_2O\uparrow$

1.2 Research methods

X-ray analysis of materials was performed using a Rigaku MiniFlex 600 diffractometer operating at 40 kV and 15 mA, equipped with a $Cu_{K\alpha}$ radiation source (λ = 0.154 nm). Diffractograms were recorded in the range of 2θ angles from 10.0º to 90.0º, the scanning speed was 1 deg/min with 0.05 deg increments. The crystallite size was calculated via following methods: the Scherrer method, the modified Scherrer method, the Williamson-Hall method, and the size-strain plot (SSP) method. Scherrer's method is based on using the formula (1) to calculate the size of the crystallites:

$$D = \frac{k \cdot \lambda}{\beta_{1/2} \cdot \cos\theta} \quad (1)$$

The modified form of Scherrer's equation is described by the formula (2):

$$\ln\beta = \ln\left(\frac{k \cdot \lambda}{D_{SM} \cdot \cos\theta}\right) = \ln\left(\frac{k \cdot \lambda}{D_{SM}}\right) + \ln\left(\frac{1}{\cos\theta}\right) \quad (2)$$

where D_{SM} – average crystallite size (nm); k – constant (k = 0.9); β – width of the peak at half-height (FWHM), measured in radians; θ – Bragg's angle; λ – wavelength of X-ray radiation (λ = 0.1546 nm). It is taken into account that the width of the peak is an integration of effects that depend on the nature of the sample and on the device. Therefore, the line broadening was estimated using the following formula (3) [33]:

$$\beta = \sqrt{[(\beta^2_{measured}) - (\beta^2_{instrumental})]}. \quad (3)$$

The size of crystallites was also calculated using Williamson-Hall (W-H) method [34]:

$$\beta \cdot \cos\theta = \frac{k \cdot \lambda}{D_{WH}} + 4\varepsilon \cdot \sin\theta, \quad (4)$$

where ε is strains.

In order to calculate the size (D) via size-strain plot method, the following formula (5) was used:

$$\left(\frac{d_{hkl}\beta\cos\theta}{\lambda}\right)^2 = \frac{K}{D_{SSP}}\left(\frac{d^2_{hkl}\beta\cos\theta}{\lambda}\right) + (2\varepsilon)^2, \quad (5)$$

where d_{hkl} – interplanar spacing, K – constant, which depends on the shape of the particles (for spherical particles K = 3/4). Interplanar spacing relates to lattice constant a and Miller indices (h, k, l) and can be calculated using the formula (6) [34]:

$$d_{hkl} = \frac{\lambda}{2\sin\theta} = \frac{a}{\sqrt{h^2+k^2+l^2}}, \quad (6)$$

Surface morphology was analyzed using scanning electron microscope REMMA-102-02 (JCS, Ukraine). Magnetic heating of the magnesium ferrite nanoparticles was studied using hand-made induction heater operating at fixed frequency of 100 kHz and regulated power up to 1 kW. The magnetic coil (5 cm in diameter) consisted of six turns of water-cooled copper pipe. Sample tube with water suspension of $MgFe_2O_4$ magnetic nanoparticles was placed in magnetic coil. The sample temperature was registered using a remote IR-thermometer. The changes of temperature depending on concentration of magnetic nanoparticles have been registered using software "Thermometer".

II. Results and discussions

2.1 X-ray analysis

X-ray diffraction provided results on the cations placement, the structure parameters of the crystal lattice of magnesium ferrite nanoparticles. The diffraction pattern of the sample was detected in the range of 2θ from 10.0º to 90.0º. As shown in Fig. 1, the peak with the highest intensity is between 35º and 37º. X-ray analysis confirmed the spinel to have a cubic structure and the magnesium ferrite to be single-phase.

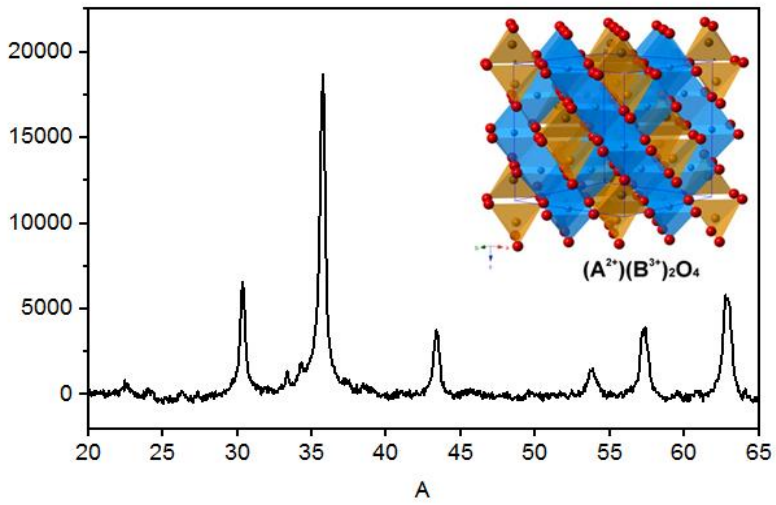

Fig. 1. Diffraction pattern of $MgFe_2O_4$ sample.

Based on the X-ray analysis data, the distribution of cations in the sublattices was obtained, and a_{th}, d_{XRD}, R_A and R_B were calculated. Theoretical lattice parameter (a_{th}) is calculated using the formula (7):

$$a_{th} = {}^{8}/_{3} \cdot \sqrt{3}(R_A + R_O) + \sqrt{3}(R_B + R_O), \quad (7)$$

where R_A i R_B – tetrahedral and octahedral radii, Å, R_O – oxygen ion radius, Å.

Tetrahedral and octahedral radii were calculated using the formulas (8)-(9):

$$R_A = c(Mg_A^{2+}) \cdot r(Mg_A^{2+}) + c(Fe_A^{3+}) \cdot r(Fe_A^{3+}), \quad (8)$$

$$R_B = [c(Mg_B^{2+}) \cdot r(Mg_B^{2+}) + c(Fe_B^{3+}) \cdot r(Fe_B^{3+})]/2, \quad (9)$$

where $c(Mg_A^{2+}), c(Fe_A^{3+})$ are ion concentrations in A-sublattice, $c(Mg_B^{2+})$, $c(Fe_B^{3+})$ are ion concentrations in B-sublattice, obtained from cation distribution.

Table 1 presents these parameters: theoretical value a_{th} equals 8.3818 Å, and experimental value a_{exp} equals 8.3820 Å. A certain correlation between a_{th} and R_A, R_B is observed: the lattice parameter increases along with increasing ionic radius. In our case, these are the radii of ions in the tetrahedral positions: $r(Mg_A^{2+}) = 0.57$ Å, $r(Fe_A^{3+}) = 0.49$ Å, and octahedral positions: $r(Mg_B^{2+}) = 0.72$ Å, $r(Fe_B^{3+}) = 0.645$ Å. As seen from the results, the radii of ions in the octahedral positions are larger in comparison with the radii of the cations Mg_B^{2+} and Fe_B^{3+} in the tetrahedral positions. The location of O^{2-} ions in the sublattices characterizes the oxygen parameter "u", which depends on the synthesis method and chemical composition of ferrite, and equals 0.375 for an ideal spinel [35]. In this case, u equals 0.431 and is close to the ideal state of oxygen ions placement in the $MgFe_2O_4$ sublattices. The X-ray density for magnesium ferrite is calculated using the formula (10):

$$d_{XRD} = \frac{8 \cdot M}{V \cdot N_a} \quad (10)$$

where M – molar mass, M ($MgFe_2O_4$) = 200 g/mol; V – cell volume (nm^3), $V = a^3$, where a – lattice parameter (nm), N_a – Avogadro constant, $N_a = 6.023 \cdot 10^{23}$ mol^{-1}. Calculation shown that d_{XRD} equals 4.51 g/cm^3. Specific surface area of spinel ferrite was calculated using the formula (11):

$$S_{XRD} = 6000/(d_{XRD} \cdot D), \quad (11)$$

where d_{XRD} – X-ray density, g/cm^3, D – crystallite size, nm.

The cationic distribution of magnesium ferrite and the inversion degree are also presented in Table 1. The inversion degree (δ) of the spinel characterizes the Fe^{3+} ions ratio in A- and B-sublattices and equals 0.786, which indicates a partially inverted structure of magnesium ferrite.

A complex of crystalchemical parameters makes it possible to determine the distances between cations (Me-Me) and cation-anion (Me-O). The image of ideal interatomic lengths and angles in the spinel structure is shown in Fig. 2.

The interatomic distances **p, q, r, s** refer to the bonds between the atoms A-B, B-B, A-A and oxygen, while **b,**

Table 1

Lattice parameter (a_{exp}), X-ray diffraction density (d_{XRD}) and cation distribution, calculated based on XRD data for $MgFe_2O_4$

a_{th}, Å	a_{exp}, Å	u	d_{XRD}, g/cm^3	V, $Å^3$	R_A, Å	R_B, Å	cation distribution	$\delta = \frac{Fe_A}{Fe_B}$
8.3818	8.3820	0.431	4.51	589	0.50	0.68	$\left(Mg_{0.12}^{2+}Fe_{0.88}^{3+}\right)_A\left[Mg_{0.88}^{2+}Fe_{1.12}^{3+}\right]_B O_4$	0.786

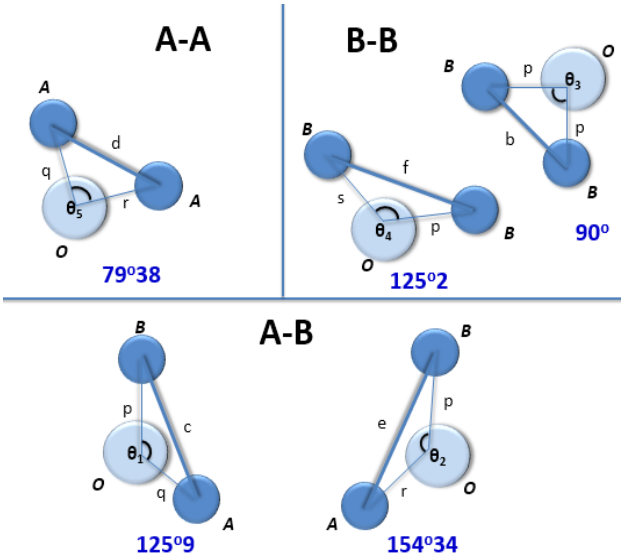

Fig. 2. The ideal interatomic lengths and angles in the spinel structure.

Table 2

Interatomic distances and angles in magnesium ferrite

Me-O	Å	Me-Me	Å	bond angle	degrees
$p = a\left(\frac{5}{8} - u\right)$	1.63	$b = \left(\sqrt{2}/4\right)$a	2.96	$\theta_1 = cos^{-1}\left(\frac{p^2 + q^2 - c^2}{2pq}\right)$	107.2
$q = a\sqrt{3}(u - \frac{1}{4})$	2.63	$c = \left(\sqrt{11}/8\right)$a	3.48	$\theta_2 = cos^{-1}\left(\frac{p^2 + r^2 - e^2}{2pr}\right)$	95.9
$r = a\sqrt{11}\left(u - \frac{1}{4}\right)$	5.03	$d = \sqrt{3}\left(a/4\right)$	3.63	$\theta_3 = cos^{-1}\left(\frac{2p^2 - b^2}{2p^2}\right)$	131.3
$s = a\sqrt{3}(\frac{u}{3} + \frac{1}{8})$	3.90	$e = \sqrt{3}\left(a/0.375\right)$	5.44	$\theta_4 = cos^{-1}\left(\frac{p^2 + s^2 - f^2}{2ps}\right)$	132.0
		$f = \sqrt{6}\left(a/4\right)$	5.13	$\theta_5 = cos^{-1}\left(\frac{r^2 + q^2 - d^2}{2rq}\right)$	43.9

c, d, e, f refer to the bonds between the metal atoms A-B, B-B and A-A. The distance **p** is between the atoms B-O, **q** - between O-A, and **c** - between A-B, together they form a hypothetical triangle BOA (pqc) with an angle $\boldsymbol{\theta_1}$, which equals 125°9 in an ideal lattice. The distance **r** is between the atoms A-O in a hypothetical triangle AOA with an angle $\boldsymbol{\theta_5}$, which equals 79°38 in an ideal lattice, where the distance between O-A = **q**, and between A-A = **d**. The angle $\boldsymbol{\theta_2}$ is in the hypothetical triangle AOB, where the distance between the metals A-B = **e**, between A-O = **r**, and between O-B = **p**. In an ideal lattice, the angle $\boldsymbol{\theta_2}$ equals 154°34. The distance **s** is between the atoms O-B in a hypothetical triangle BOB with an angle $\boldsymbol{\theta_4}$, which equals 125°2 in an ideal lattice, where the distance between B-O = **p**, and between B-B = **f**. The angle $\boldsymbol{\theta_3}$ is in a hypothetical isosceles triangle BOB, where the distance between the metals B-B equals **b**, and the distance between B-O = O-B = **p**. In an ideal lattice, the angle $\boldsymbol{\theta_3}$ equals 90° [36].

Based on the experimental lattice parameter, as well as the oxygen parameter, the interatomic distances and angles in the primitive cell of magnesium ferrite were obtained, which are presented in Table 2. The Me-O distances are observed to have smaller values (in the range of 1.63 - 5.03 Å) compared to Me-Me distances (2.96 - 5.44 Å). Accordingly, this means that there must be a stronger interatomic bond between the metal cations and the oxygen anions, because the distance between them is smaller. The calculated angles θ_1 and θ_4 are close to ideal, in our case they equal 107.2° and 132.0°, respectively (they equal 125°9 and 125°2 in an ideal lattice). The angles θ_2 (95.9°) and θ_3 (131.3°) have slight deviations, greater than ideal values; θ_5 is 43.9° and is less than the value of the same angle in an ideal lattice.

The crystallite size has a great influence on the spinel properties. There is a tendency: the smaller the size of crystallites in ferrites, the better the optical, photocatalytic and adsorption characteristics [18]. In order to estimate the average crystallite size of magnesium ferrite, the following methods were used: a modified Scherrer method ($(\ln(\beta_{1/2})–\ln(1/\cos\theta)$), Williamson-Hall method ($\beta_{1/2}\cos\theta–4\sin\theta$) and SSP method ($(d\cdot\beta\cdot\cos\theta/\lambda)^2–d^2\cdot\beta\cdot\cos\theta/\lambda$), as shown in Fig. 3.

Based on the correlation coefficient values, we can conclude that SSP method is best suited for the calculation of crystallite size, as R^2 equals 0.989 and has the highest value compared to other methods. The spinel size varies from 11 nm (SSP) to 20 nm (W-H). The crystallite size also affects the value of $MgFe_2O_4$ surface area, meaning high S_{XRD} (which is in the range of 68 - 125 m^2/g in our case) is due to relatively small size of the crystallites. The strains (ε) and dislocation density (δ) are additionally calculated from the slope of the line in Williamson-Hall method, the values of which are $0{,}275\cdot10^{-3}$ and 0.0026 respectively. The same parameters were estimated using size-strain plot method: $\varepsilon = 4.472\cdot10^{-3}$, $\delta = 0.0045$.

2.2 Scanning electron microscopy

For morphological study of ferrite nanoparticles, scanning electron microscopy was used. The SEM image of $MgFe_2O_4$, synthesized via sol-gel auto-combustion method with honey (a natural reducing agent), is shown in Fig. 4. The average agglomerate particle size appears to be 20 μm. It is assumed that agglomeration in ferrites occurs due to their magnetic nature [37]. The spinel is observed to have a dense arrangement of almost spherically shaped particles with pronounced pores. Such pores can occur during synthesis due to the release of CO_2 and N_2 gases.

2.3 Magnetic hyperthermia

For a more detailed study, hyperthermic properties of magnesium ferrite were analyzed, being potentially usable in medicine for destruction of cancer cells. In magnetic hyperthermia, nanoparticles, which are able to heat up to a certain temperature under an external magnetic field, are used. In our case, the results of this study are presented in Fig. 5. It shows the dependence of the heating temperature for different amounts of $MgFe_2O_4$ (50; 75; 100 mg) on the heating time. As can be seen from Fig. 5, during 40 min the heating temperature of three samples of ferrite increases to 32, 36 and 46 °C, respectively. The 100 mg/ml sample of magnesium ferrite is observed to reach the appropriate range of hyperthermia – 42 – 46 °C, in which the

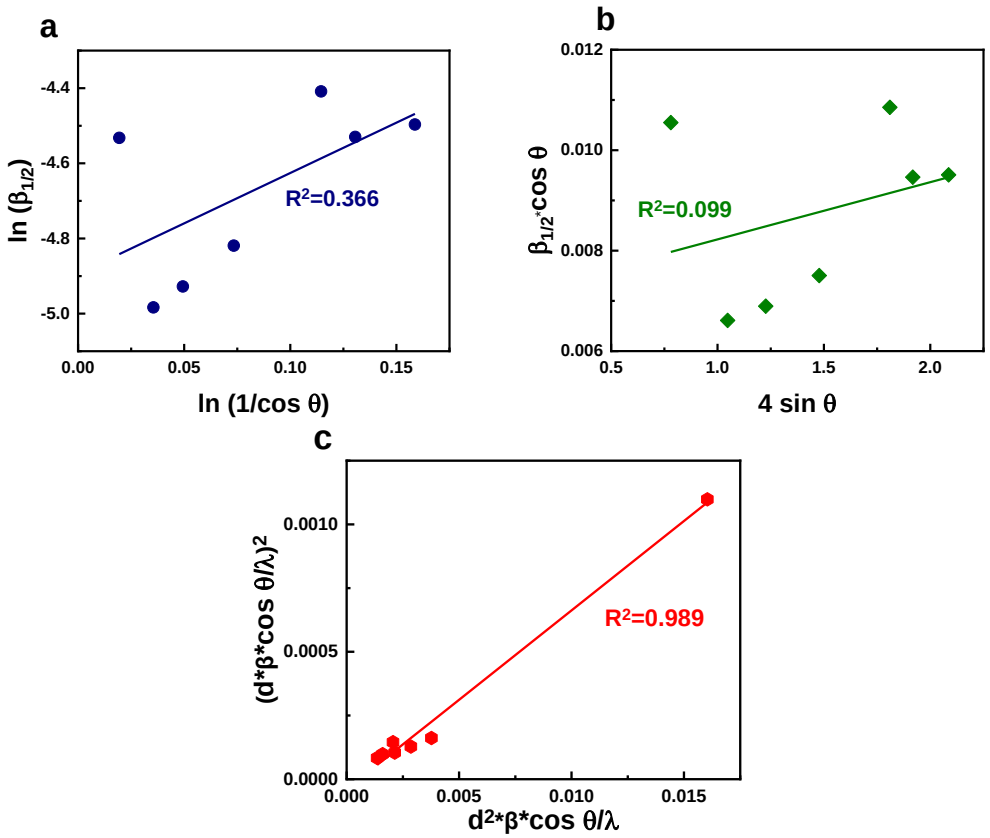

Fig. 3. Estimation of the crystallite size of magnesium ferrite using modified Scherrer method (a), Williamson-Hall method (b) and SSP method (c).

Table 3

Crystallite sizes (D), strains (ε), dislocation density (δ) and surface area (S_{XRD}) for magnesium ferrite, calculated using Scherrer method (SM), Williamson-Hall method (WH) and size-strain plot method (SSP)

method	crystallite size D, nm	strains, $\varepsilon \cdot 10^{-3}$	dislocation density (δ)	surface area S_{XRD}, m^2/g
Scherrer	16	-	0.0037	81
modified Scherrer	19	-	0.0029	72
Williamson-Hall	20	0.275	0.0026	68
size-strain plot	11	4.472	0.0045	125

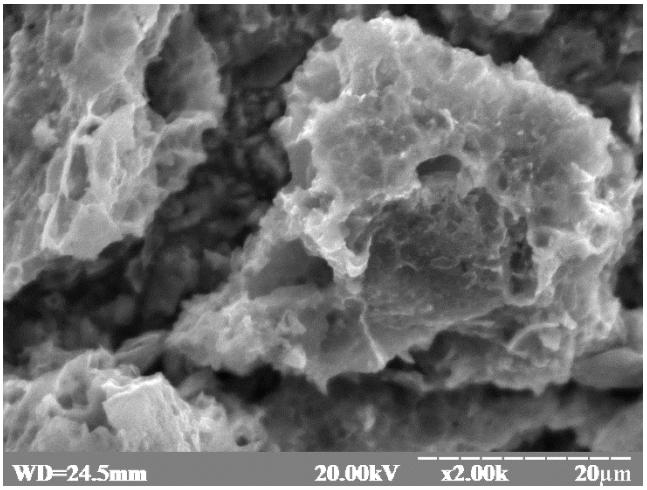

Fig. 4. Scanning electron microscopy of magnesium ferrite.

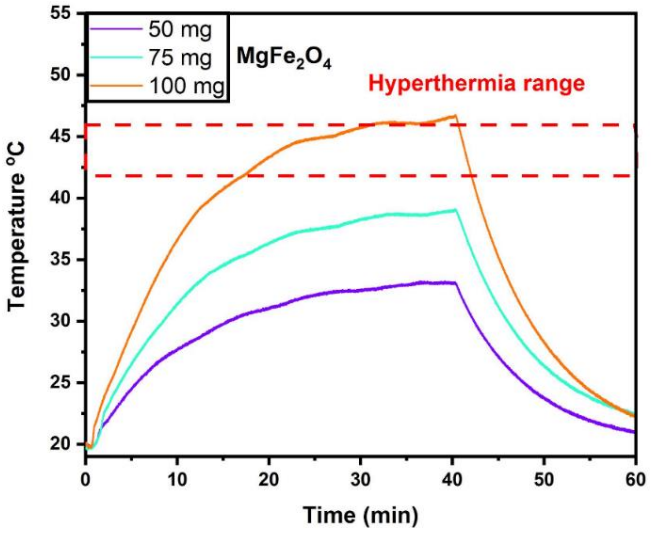

Fig. 5. Hyperthermic properties of magnesium ferrite.

destruction of cancer cells is activated. Samples with less $MgFe_2O_4$ content were being heated to the range of 25 - 35 °C. As a result, the heating temperature increased along with increasing portion of ferrite. Therefore, in this case, a 100 mg spinel $MgFe_2O_4$ sample can be heated to the desired temperature, which will increase the sensitivity of cancer cells and provide a characteristic therapeutic effect.

Conclusions

Spinel nanoparticles of magnesium ferrite were synthesized via sol-gel autocombustion method using honey as a reducing agent. X-ray diffraction was used to describe the structure of the crystal lattice, the size of the crystallites, and the location of the cations of given nanomaterial, which confirmed the spinel to have a cubic structure and the magnesium ferrite to be single-phase. The theoretical lattice parameter was calculated, equaling 8.3818 Å. The oxygen parameter of the lattice was also determined, which equals 0.431 and is close to the ideal state of placement of O^{2-} ions in $MgFe_2O_4$. The cationic distribution is expressed by the formula $\left(Mg^{2+}_{0.12}Fe^{3+}_{0.88}\right)_A\left[Mg^{2+}_{0.88}Fe^{3+}_{1.12}\right]_BO_4$, and the inversion degree indicates the almost inverse structure of magnesium ferrite. In addition, the interatomic distances and angles in the spinel were calculated, also being close to the ideal lattice. Crystallite sizes were estimated using the modified Scherrer method, Williamson-Hall method and size-strain plot (SSP) method. The average size of the spinel varies from 11 nm (size-strain plot method) to 20 nm (Williamson-Hall method). SEM microphotography characterized the morphology of the ferrite surface with a dense arrangement of particle agglomerates with a porous structure. Analysis of the hyperthermic properties of magnesium ferrite showed that a 100 mg sample of spinel $MgFe_2O_4$ can provide destruction of cancer cells in the temperature range of 42 – 46 °C. Therefore, due to its structural, magnetic and hyperthermic properties, the study of spinel magnesium ferrite is important in various fields of application.

Acknowledgements

Financial support of this work was obtained from Ministry of Education and Science of Ukraine (project number 0118U000258).

Tatarchuk T. – PhD in Chemistry, Associate Professor of the Chemistry Department, Director of Educational and Scientific Center of Materials Science and Nanotechnology;
Myslin M. – MSc, senior laboratory assistant of the Chemistry Department;
Lapchuk I. – 4th year student, Chemistry Department;
Olkhovyy O. – 4th year student, Faculty of Pharmacy;
Danyliuk N. – MSc, leading specialist at the Educational and Scientific Center of Materials Science and Nanotechnology;
Mandzyuk V. – DSc in Physics and Mathematics, Associate Professor of the Department of Computer Engineering and Electronics.

[1] S. Gul, M.A. Yousuf, A. Anwar, M.F. Warsi, P.O. Agboola, I. Shakir, M. Shahid, Ceram. Int. 46, 14195 (2020) (doi:10.1016/j.ceramint.2020.02.228).
[2] K.K. Kefeni, T.A.M. Msagati, B.B. Mamba, Mater. Sci. Eng. B. 215, 37 (2017) (doi:10.1016/J.MSEB.2016.11.002).

[3] D.H.K. Reddy, Y.-S. Yun, Coord. Chem. Rev. 315, 90 (2016) (doi:10.1016/J.CCR.2016.01.012).
[4] N. Deng, L. Zhou, X. Peng, X. Wang, H. Ge, Xiyou Jinshu Cailiao Yu Gongcheng/Rare Met. Mater. Eng. 44, 2126 (2015) (doi:10.1016/s1875-5372(16)30010-8).
[5] M. Amiri, M. Salavati-Niasari, A. Akbari, Adv. Colloid Interface Sci. 265, 29 (2019) (doi:10.1016/J.CIS.2019.01.003).
[6] K.K. Kefeni, B.B. Mamba, T.A.M. Msagati, Sep. Purif. Technol. 188, 399 (2017) (doi:10.1016/J.SEPPUR.2017.07.015).
[7] S. Bindra Narang, K. Pubby, J. Magn. Magn. Mater. 167163 (2020) (doi:10.1016/j.jmmm.2020.167163).
[8] K. Shetty, H.P. Nagaswarupa, D. Rangappa, K.S. Anantharaju, B.S. Surendra, A. Kumar, Mater. Today Proc. 5, 22362 (2018) (doi:10.1016/j.matpr.2018.06.603).
[9] N. Sivakumar, S.R.P. Gnanakan, K. Karthikeyan, S. Amaresh, W.S. Yoon, G.J. Park, Y.S. Lee, J. Alloys Compd. 509, 7038 (2011) (doi:10.1016/j.jallcom.2011.03.123).
[10] K.W. Jung, S. Lee, Y.J. Lee, Bioresour. Technol. 245, 751 (2017) (doi:10.1016/j.biortech.2017.09.035).
[11] R.P. Singh, C. Venkataraju, Chinese J. Phys. 56, 2218 (2018) (doi:10.1016/j.cjph.2018.07.005).
[12] A. Meidanchi, A. Motamed, Preparation, characterization and in vitro evaluation of magnesium ferrite superparamagnetic nanoparticles as a novel radiosensitizer of breast cancer cells, Ceram. Int. 46 (2020) 17577–17583. doi:10.1016/j.ceramint.2020.04.057.
[13] T. Tatarchuk, M. Bououdina, J.J. Vijaya, L.J. Kennedy, Nanomater. Interface Stud. Appl. Proc. Phys. 195, 305 (2017) (doi:10.1007/978-3-319-56422-7).
[14] K.S. Lee, H.J. Bang, S.T. Myung, J. Prakash, K. Amine, Y.K. Sun, J. Power Sources. 174, 726 (2007) (doi:10.1016/j.jpowsour.2007.06.110).
[15] X. Zhang, Z. Chen, C. Wu, J. Zhang, F. Wang, Chem. Phys. Lett. 732, 136647 (2019) (doi:10.1016/j.cplett.2019.136647).
[16] A.A. Rodríguez-Rodríguez, M.B. Moreno-Trejo, M.J. Meléndez-Zaragoza, V. Collins-Martínez, A. López-Ortiz, E. Martínez-Guerra, M. Sánchez-Domínguez, SInt. J. Hydrogen Energy. 12421 (2019) (doi:10.1016/j.ijhydene.2018.09.183).
[17] T. Karpova, V. Vassiliev, E. Vladimirova, V. Osotov, M. Ronkin, A. Nosov, Ceram. Int. 38, 373 (2012) (doi:10.1016/j.ceramint.2011.07.016).
[18] T. Tatarchuk, M. Myslin, I. Mironyuk, M. Bououdina, A.T. Pędziwiatr, R. Gargula, B.F. Bogacz, P. Kurzydło, J. Alloys Compd. 819, 152945 (2020) (doi:10.1016/J.JALLCOM.2019.152945).
[19] E. Mazario, M.P. Morales, R. Galindo, P. Herrasti, N. Menendez, J. Alloys Compd. 536, S222 (2012) (doi:10.1016/j.jallcom.2011.10.073).
[20] R. Singh Yadav, I. Kuřitka, J. Vilcakova, T. Jamatia, M. Machovsky, D. Skoda, P. Urbánek, M. Masař, M. Urbánek, L. Kalina, J. Havlica, Ultrason. Sonochem. 61, 104839 (2020) (doi:10.1016/j.ultsonch.2019.104839).
[21] P. Mondal, A. Anweshan, M.K. Purkait, Chemosphere 259, 127509 (2020) (doi:https://doi.org/10.1016/j.chemosphere.2020.127509).
[22] B.A. de Marco, B.S. Rechelo, E.G. Tótoli, A.C. Kogawa, H.R.N. Salgado, Saudi Pharm. J. 27, 1 (2019) (doi:10.1016/j.jsps.2018.07.011).
[23] P. Gómez-López, A. Puente-Santiago, A. Castro-Beltrán, L.A. Santos do Nascimento, A.M. Balu, R. Luque, C.G. Alvarado-Beltrán, Curr. Opin. Green Sustain. Chem. 24, 48 (2020) (doi:10.1016/j.cogsc.2020.03.001).
[24] U.P. Manik, A. Nande, S. Raut, S.J. Dhoble, Results Mater. 6, 100086 (2020) (doi:10.1016/j.rinma.2020.100086).
[25] T.B. Vidovix, H.B. Quesada, E.F.D. Januário, R. Bergamasco, A.M.S. Vieira, Mater. Lett. 257, 126685 (2019) (doi:10.1016/j.matlet.2019.126685).
[26] G. Maheshwaran, A. Nivedhitha Bharathi, M. Malai Selvi, M. Krishna Kumar, R. Mohan Kumar, S. Sudhahar, J. Environ. Chem. Eng. 8, 104137 (2020) (doi:10.1016/j.jece.2020.104137).
[27] N. Thangamani, N. Bhuvaneshwari, Chem. Phys. Lett. 732, 136587 (2019) (doi:10.1016/j.cplett.2019.07.015).
[28] J.A.A. Abdullah, L. Salah Eddine, B. Abderrhmane, M. Alonso-González, A. Guerrero, A. Romero, Sustain. Chem. Pharm. 17, (2020) (doi:10.1016/j.scp.2020.100280).
[29] M. Ramzan, R.M. Obodo, S. Mukhtar, S.Z. Ilyas, F. Aziz, N. Thovhogi, Mater. Today Proc. (2020) (doi:10.1016/j.matpr.2020.05.472).
[30] G. Theophil Anand, D. Renuka, R. Ramesh, L. Anandaraj, S. John Sundaram, G. Ramalingam, C.M. Magdalane, A.K.H. Bashir, M. Maaza, K. Kaviyarasu, Surfaces and Interfaces. 17, 100376 (2019) (doi:10.1016/j.surfin.2019.100376).
[31] R.S. Yadav, I. Kuřitka, J. Vilcakova, P. Urbánek, M. Machovsky, M. Masař, M. Holek, J. Phys. Chem. Solids. 110, 87 (2017) (doi:https://doi.org/10.1016/j.jpcs.2017.05.029).
[32] P. Laokul, V. Amornkitbamrung, S. Seraphin, S. Maensiri, Curr. Appl. Phys. 11, 101 (2011) (doi:10.1016/j.cap.2010.06.027).
[33] A. Khorsand Zak, W.H. Abd. Majid, M.E. Abrishami, R. Yousefi, Solid State Sci. 13, 251 (2011) (doi:10.1016/J.SOLIDSTATESCIENCES.2010.11.024).
[34] R. Kumar, M. Kar, J. Magn. Magn. Mater. 416, 335 (2016) (doi:10.1016/j.jmmm.2016.05.035).

[35] M.I. Arshad, S. Arshad, K. Mahmood, A. Ali, N. Amin, Umaid-ur-Rehman, M. Isa, A. Akram, N. Sabir, M. Ajaz-un-Nabi, Phys. B Condens. Matter. 599, 412496 (2020) (doi:10.1016/j.physb.2020.412496).
[36] T.R. Tatarchuk, M. Bououdina, N.D. Paliychuk, I.P. Yaremiy, V.V Moklyak, J. Alloys Compd. 694, 777 (2017) (doi:10.1016/j.jallcom.2016.10.067).
[37] P. Aji Udhaya, T.C. Bessy, M. Meena, Mater. Today Proc. 8, 169 (2019) (doi:10.1016/j.matpr.2019.02.096).

Т. Татарчук[1], М. Мислін[1], І. Лапчук[1], О. Ольховий[2], Н. Данилюк[1], В. Мандзюк[1]

Синтез, структура і морфологія наночастинок фериту магнію, синтезованих «зеленим» методом

[1]*Прикарпатський національний університет імені Василя Стефаника, Івано-Франківськ, Україна,* tatarchuk.tetyana@gmail.com
[2]*Ягеллонський університет, Краків, Польща,* oolkhovyi@gmail.com

У роботі синтезовано наночастинки шпінельного магній фериту ($MgFe_2O_4$), описано його структурні, морфологічні та гіпертермічні параметри, що забезпечують ефективне використання в різних областях. Ферит магнію синтезували за допомогою золь-гель методу автогоріння, використовуючи мед як відновник. Розмір кристалітів розраховували за методом Шеррера, модифікованим методом Шеррера, методом Вільямсона-Холла та розмірно-деформаційним методом. Для підтвердження структури шпінелі використовували Х-променевий аналіз. Для морфологічного дослідження наночастинок фериту застосовували скануючу електронну мікроскопію. Проаналізовано гіпертермічні властивості фериту магнію щодо його можливого використання в медицині. Відповідно до отриманих даних, наночастинки шпінельного фериту магнію виявилися придатними для знищення ракових клітин, оскільки їх можна нагрівати до температури 42 - 46ºС, яка збільшує чутливість цих клітин.

Ключові слова: шпінель, магній ферит, наночастинки, «зелений синтез», магнітна гіпертермія.